Effect of the shape of footing on bearing capacity

Effet de la forme du pied sur la capacité portante

M.S.A.Siddiquee – *CE Department, BUET, Dhaka, Bangladesh*
F.Tatsuoka – *IIS, The University of Tokyo, Japan*
T.Tanaka – *Meiji University, Japan*

ABSTRACT: This paper explains the effects of shape of footing on its bearing capacity and settlement of footing on sand. This study involves physical model test of varying footing shapes and numerical simulation of those footings with the same material properties as the model tests. Material model is a isotropically strain hardening elasto-plastic model with non-associated flow rule. The model includes the effects induced as well as inherent anisotropies. It included pressure sensitivity and softening with shear banding. A series of physical model tests were performed using two large footing width B_0=23 cm and B_0=10 cm resting on sands having different densities and length of footing at PWRI, Tsukuba, Japan. Bearing capacity of a footing increases sharply as the B/L ratio increases from zero. There exists an optimum ratio of B/L for which bearing capacity of a rectangular footing can be maximized. The semi-empirical formula, given by de-Beer (1970) and Meyerhof (1963) are successfully explained.

RESUME: Ce papier explique de effets de forme de pieds à capacité palier et tassement de pied sur le lit à sable. La étude comporte l'épreuve de modèle physique de forme de pieds différent et simulation numérique de les pieds à la même propriété matériel aussi l'épreuve de modèle phyisique. Un modèle matériel est développé âtre adapté le type de analyse que est un analyse à trois dimensions essentiellement. Le modèle matériel est un modèle de strain dureissement élastique plastique avec la règles de écoulement non associé.'Le modèle comprendt les effets amené comme anisotropique inhérent. Il comprendé sensibilité à pressionet amollissement avec bande à cisaillement. Une étude expérimental étendu été poursuivé à PWRI, Tsukuba, Japan. Des épreuve de modèle physique en série été fait avec deux pieds large à B_0=23 cm et B_0=10 cm de largeur sur le lit à sable avec densité différent et longueur de pied.

1 INTRODUCTION

This paper explains the effects of shape of footing on its bearing capacity and settlement of footing on sand. Most of the previous studies of the effect of the shape of footing on its bearing capacity found in the literature of Soil Mechanics are not comprehensive . This study involves physical model test of varying footing shapes and numerical simulation of those footings with the same material properties and loading condition as the model tests. In doing so, a material model is developed to suit the type of analysis which is essentially a three-dimensional analysis. This three-dimensional material model is an extension of the 2D material model (Tatsuoka and Siddiquee et al.,1994). The 2D material model is a isotropically strain hardening elasto-plastic model with non-associated flow rule. The model includes realistically post-peak softening behaviour through mesh size dependent smear-crack model (Siddiquee, et al., 1995). The model includes the effects induced as well as inherent anisotropies. The model is developed basically for 2D plane strain analysis and consequently, the influence of intermediate principal stress (σ_2) is ignored. But in a 3D material model, the effect of intermediate principal stress (σ_2) will be pronounced and at the same time the anisotropy due to the bedding plane orientation will have more angle parameters due to 3D-orientation. These are the major modifications of the 2D material model carried out to perform a 3D analysis on a 3D material model.

Extensive experimental study was carried out at PWRI, Tsukuba, Japan. A series of physical model tests were performed using two large footing width B_0=23 cm and B_0=10 cm resting on sands having different densities and length. B/L were 0.0, 0.25, 0.50, 0.74 and 1.0. It was very difficult to reproduce identical densities for such a huge sand pit. So the results were obtained for different densities and those results were corrected for density variation. A FEM simulation is carried out using a mesh of 1000 nodes and 8 noded brick elements. B/L are varied in order on 0.0373, 0.0575, 0.125, 0.167,0.25,0.5,0.74,1.0 for both B_0=23 cm and B_0=10 cm.

It has been found that bearing capacity of a footing increase sharply as the ratio B/L increases from zero (plane strain case). There exists an optimum ratio of B/L for which bearing capacity of a rectangular footing can be maximized. The full variation of shape factors with B/L is traced. Opposite trend of semi-empirical formula, given by de-Beer (1970) and Meyerhof (1963) is successfully explained.

2 REVIEW

The footing size, orientation and position relative to the ground surface have an influence on the bearing capacity of foundation. This has been investigated both theoretically and experimentally by a number of researchers, namely, Brinch Hansen (1970) and Meyerhof (1963). The factors are summarized in the following Table 1.

Table 1 Different shape factors

Author	S_q	S_γ
Meyerhof as modified by Vesic	$S_q = S_\gamma = 1 + 0.1 N_\varphi \frac{B}{L}$	$S_\gamma = S_q$
Brinch Hansen as modified by Vesic	$1 + \frac{B}{L}\tan\varphi$	$1 - 0.4\frac{B}{L}$

3 MATERIAL MODEL

The material model is a generalized elasto-plastic, isotropic strain hardening-softening one with shear banding. A generalized hyperbolic equation (Tatsuoka and Siddiquee et al., 1994) has been used as the growth function of the yield surface. The yield surface used is a generalized Mohr-Coulomb one given by;

$$\Phi = \eta I_1 + \frac{1}{g(\theta)}\sqrt{J_2} - K \qquad (1)$$

, where I_1 is the first invariant of stress (i.e. hydrostatic stress component) , J_2 is the second invariant of deviatoric stress and $g(\theta)$ is the Lode angle function which is defined as;

$$g(\theta) = \frac{3 - \sin\phi_{mob}}{2\sqrt{3}\cos\theta - 2\sin\theta\sin\phi_{mob}} \quad (2)$$

η is the deviatoric stress at θ=30° (on the π-plane), which is related to the mobilized angle of internal friction ϕ_{mob} as;

$$\eta = \frac{2\sin\phi_{mob}}{\sqrt{3}(3 - \sin\phi_{mob})} \quad (3)$$

The plastic potential is defined as;

$$\Psi = \alpha' I_1 + \sqrt{J_2} - K = 0 \quad (4)$$

This equation of plastic potential is Drucker-Prager type, and similar to that of yield surface except the difference in that $g(\theta)=1.0$ in Eq. (1). This equation was employed so as to have differentiability at all stress-states. The factor α' depends on the type of analysis. As all the analysis was done under plane strain conditions in the present study, the factor α' used was;

$$\alpha' = \frac{\tan\psi}{\sqrt{9 + 12\tan^2\psi}} \quad (5)$$

, where ψ is the mobilized angle of dilatancy, which is given by;

$$\psi = \arcsin\left(-\frac{d\varepsilon_1^p + d\varepsilon_3^p}{d\varepsilon_1^p - d\varepsilon_3^p}\right) \quad (6)$$

, where $d\varepsilon_1^p$ and $d\varepsilon_2^p$ are the major and minor principal strain increments (positive in compression). In this study, the value of ψ was determined from Rowe's stress dilatancy relation

$$\frac{\sigma_1}{\sigma_3} = -K\left(\frac{d\varepsilon_1^p}{d\varepsilon_3^p}\right) \quad (K = \text{a material constant}) \quad (7)$$

As the model has the yield function and plastic potential surface having different forms, it is one of the non-normal plasticity models, or in other words it is a non-associated flow model.

4 FEM DETAILS

Four noded quadrilateral elements with reduced integration was used. An anti-hourglass scheme was used to prevent any probable hour-glass mode. The systems of nonllinear equations are solved by Dynamic Relaxation (DR) technique (Siddiquee et al., 1995), which has reputation in solving highly nonlinear equation specially for high friction angle materials (i.e., dense Toyoura sand, having an angle of internal friction=50°)

The integration of the elasto-plastic equation was done by the return mapping scheme. Localization is captured by using a mesh size dependent hardening modulus. This is achieved by introducing a localization parameter S in the additive decomposition of total strain increment as follows,

$$d\varepsilon_{ij} = d\varepsilon_{ij}^e + S d\varepsilon_{ij}^p \quad (8)$$

where, $S = F_b / F_e$, where F_b is the area of the shear band in one element and F_e is the area of the element. In this way of calculation S actually becomes,

$$S = \frac{W}{n\sqrt{F_e}} \quad (9)$$

where, W is the width of shear band, n is the number of Gauss points for integration.

It is assumed from experimental observations in plane strain compression tests that the deformation is homogeneous up to the peak stress state, while strain localization into a shear band starts at the peak stress state. In this analysis, convergence was checked by checking the global residual force norm and the differential residual force norm between two successive iterations. In this analysis, all computations were made, based on tolerances, $\varepsilon_1 = \varepsilon_2 = 10^{-6}$

4.1 *Experimental data and correction*

A series of costly experiments were carried out at PWRI, Tsukuba, Japan by using two large footing with B_0=23 cm and B_0=10 cm resting on sands having different densities. It is very difficult to reproduce a very identical density for a large sand pit. The results of experiment are given in the following charts (Table 2 and 3). Note that one test or two tests for different B/L were performed for each sand bed.

Table 2 Model test results of B_0=23 cm.

Case no.	B x L (cmx cm)	B/L	Den sity (gm/cc)	q_u^* (t/m²)	$2q_u/\gamma B$	Cor. $2q_u/\gamma B$	S_f/B (%)	Cor. S_f/B (%)
1	23 x 23	1.0	1.515	30.85	177	359.63	9.66	7.86
2	23 x 31	0.74	1.515	31.17	179	363.70	10.11	8.23
3	23 x 46	0.50	1.540	33.86	191	284.46	9.28	8.05
4	23 x 23	1.0	1.524	26.05	149	267.09	12.30	10.24
5	23 x 31	0.74	1.524	27.90	159	285.02	12.24	10.19
14	23 x 23	1.0	1.566	38.1	212	250.21	10.75	10.01
15	23 x 31	0.75	1.586	42.4	232	237.90	11.00	10.86
16	23 x 46	0.50	1.571	44.8	248	281.86	11.0	10.39
17	23 x 92	0.25	1.592	34.0	186	183.73	7.37	7.41

* the peak value of average footing pressure.

Table 3 Model test results of B_0=10 cm.

Case no.	B x L (cm x cm)	B/L	Den sity (gm/cc)	q_u^* (t/m²)	$2q_u/\gamma B$	Cor. $2q_u/\gamma B$	S_f/B (%)	Cor S_f/B (%)
6	10 x 10	1.0	1.519	16.40	216	414.17	9.23	7.59
7	10 x 40	0.25	1.519	15.08	199	381.58	6.48	5.32
8	10 x 13.5	0.74	1.545	15.04	195	276.16	9.61	8.45
9	10 x 20	0.5	1.545	15.20	197	279.00	9.64	8.47
10	10 x 10	1.0	1.528	12.20	160	272.74	9.18	7.72
11	10 x 40	0.25	1.528	15.80	207	352.86	5.85	4.92
12	10 x 10	1.0	1.531	19.4	253	416.08	8.25	6.99
13	10 x 13.3	0.75	1.554	21.8	281	366.14	9.87	8.89

From the above Table 2 and 3, it is clear that the results $N_\gamma=(2q/\gamma B)_{max}$ varied due to the variation of density of sand pit among the different tests cases. So, an intuitive method of correction is applied. From the results of plane strain model tests on different sand densities with B_0=10 cm performed by Tani (1988), a correlation was obtained as follows (Figs. 1 and 2),

$$N_\gamma = -4994.835 + 5437.38 \times \gamma_d - 1375.95 \times \gamma_d^2 \quad (10)$$

$$S_f / B_0 = 0.32096 - 0.16726 \times \gamma_d \quad (11)$$

where,

γ_d= the dry density of sand, N_γ= the bearing capacity factor, S_f / B = the relative settlement at peak footing load.

Using the rate of change (the slopes of equations) of Eqs. 10 and 11, the results of those bearing capacity tests done with rectangular footings on Toyoura sand (Tables. 2 and 3) are transformed to the target density (=1.59 gm/cm³). The transformation used as follows,

$$\frac{N_\gamma}{N'_\gamma} = \frac{-4994.835 + 5437.38 \times (1.59) - 1375.95 \times (1.59)^2}{-4994.835 + 5437.38 \times \gamma'_d - 1375.95 \times \gamma'^2_d} \quad (12)$$

$$\frac{S_\gamma}{B_0} = \frac{0.32096 - 0.16726 \times (1.59)}{0.32096 - 0.16726 \times \gamma'_d}\left(\frac{S_\gamma}{B_0}\right)' \quad (13)$$

where,

γ'_d= the dry density of the sand bed on which the rectangular footing test was performed, which is different from 1.59 gf/cm³.

N'_γ= the measured bearing capacity factor in the rectangular footing test. $(S_f / B)'$= the measured relative settlement at the peak footing load in the rectangular footing test.

The following discussions on this topic refer to all the corrected bearing capacity factors and footing settlement of rectangular footings.

4.2 *FEM simulation of the effect of footing shape*

The FEM simulations of the effect of footing shape are carried out by performing three dimensional FEM analysis. The meshes shown in Fig. 3 each consists of 1000 nodes. The ratio of B/L are varied in the order of 1.0, 0.74, 0.50, 0.25, 0.167, 0.125, 0.0575, 0.0373 for both B_0=23 cm and B_0=10 cm. Loading is applied by a constant rate of footing displacement (0.2B/500 cm/step). The boundary conditions on the boundary sides are all rollers.

Figs. 4 and 5 show the relationship between the normalized footing pressure and the relative settlement for all the cases of footing width and length under consideration. It is acutely noticeable that the failure-modes are **local failures** as observed from these load-displacement curves. And as the ratio B/L goes closer to 0.0 (plane strain condition), the modes of failure changes to a general type of failure showing a definite peak. It is clear from the observation of Figs. 4 and 5 that as B/L increases from 0.0 (plane strain), the peak value N becomes less clear in that after the yield point in the N~S/B relation, the N value still tends to increase. This result suggests that in the 3D case (i.e., B/L > 0.0) the failure of ground outside the footing area is more progressive than in the plane strain case. In the case of B/L > 0.0, the post-peak curves never fall abruptly approaching to the residual strength as it goes in the case of plane strain cases of strip footing. This is the case even for the ratio, B/L gets closer to plane strain case (B/L=0.0). This may be attributed to the different way of strain localization in the ground. In a three-dimensional situation the formation of shear band by strain localization is still controvertial since the observation of the ground failure in 3D bearing capacity tests is extremely difficult. However, it can be said definitely that the failure mechanism of ground is not the same between 2D and 3D cases.

Fig. 6 compares the bearing capacity factors N_γ from the FEM analysis and those from the model tests for B_0=23 cm. A similar result for B_0=10 cm is shown in Fig.7. It can be noticed that the model tests show a result having a little scattering in it. The results of the FEM simulation are quite close to the experimental results in the sense that both has a tendency of increasing the bearing capacity very fast with the increase in the ratio B/L as B/L increases from 0.0 to a certain value and afterward it becomes almost constant. This result suggests that there is an optimum smallest B/L ratio for which it gives the maximum bearing capacity. It may also be noted that the bearing capacity factors from FEM simulations overestimate the bearing capacity from the model tests to a larger extent as B/L increases from 0.0; this is particularly the case for B_0=10 cm.. The reason may be larger-sized elements relatively to B_0 employed in the analysis of B_0=10 cm footing. But the tendency of the bearing capacity N_γ to increase with the increase in B/L is also reflected in even this case.

Figs. 8 and 9, respectively for B_0=23 cm and 10 cm show the relationships between the normalized values of N_γ obtained by being divided with the value at B/L=0.0 (plane strain case). The normalization is done to compare the results of model test and FEM simulation with the existing theoretical and empirical expressions (Meyerhof, 1963). First one is an semi-empirical one proposed by de Beer (1970) based on his small-scale model tests in 1g, which was later quoted by, Vesic (1973),

$$S_\gamma = 1 - 0.4\frac{B}{L} \qquad (14)$$

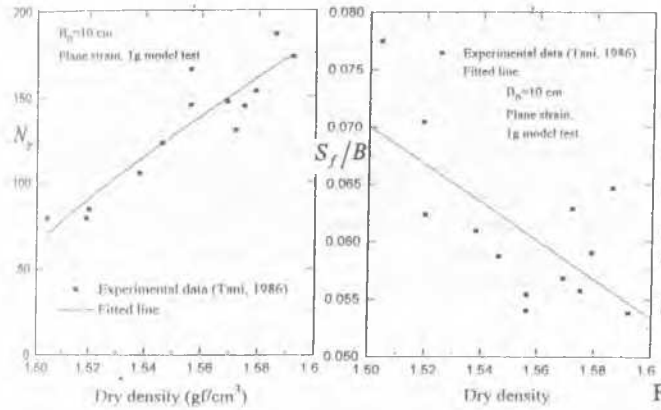

Fig. 1 Regression of N_γ with density.

Fig. 2 Regression of S_f/B with density.

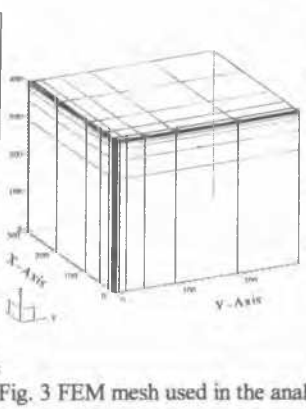

Fig. 3 FEM mesh used in the analysis.

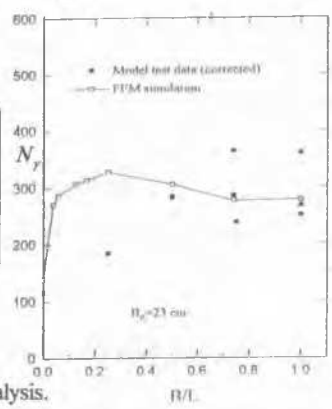

Fig. 6 Comparison of model test results with FEM (B_0=23 cm).

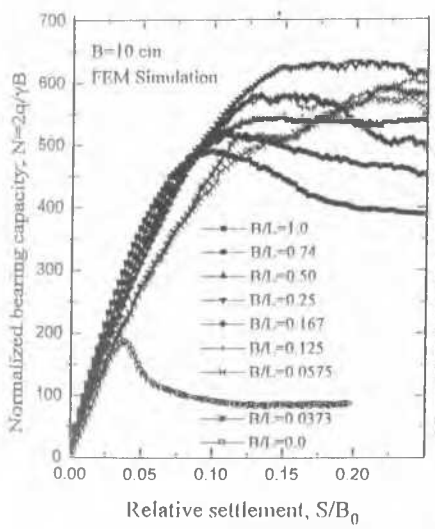

Fig. 4 Normalized load vs. relative settlement for B_0=10 cm.

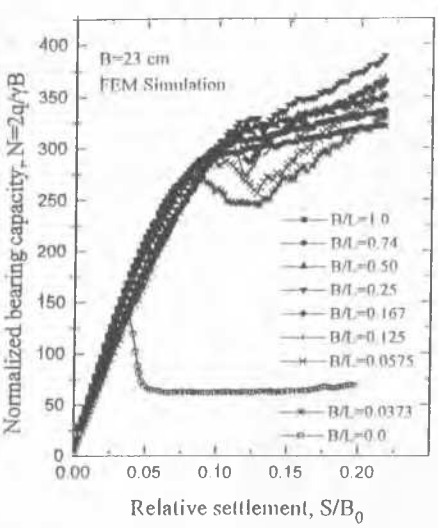

Fig. 5 Normalized load vs. relative settlement for B_0=23 cm.

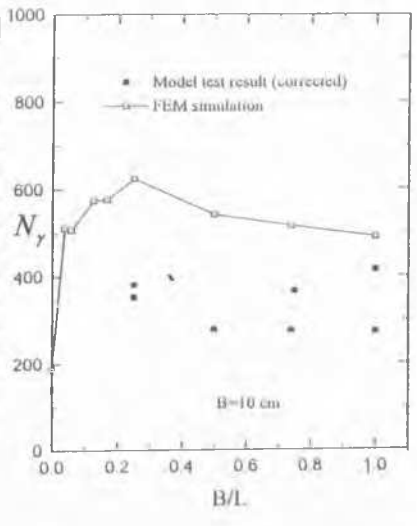

Fig. 7 Comparison of model test results with FEM (B_0=10 cm)

Another is a semi-empirical one given by Meyerhof (1963),

$$S_\gamma = 1 + 0.1 N_\varphi \frac{B}{L} \qquad (15)$$

where, N_φ is a factor defined elsewhere

These relations shows quite oposite tendencies in the variation of shape factor with B/L.The comparison shown in Figs. 8 and 9 invalidates the relation of Eq. 14 provided by de Beer (1970). Actually, he tested for b/l=1/6 to 1 and extended the results to the plane strain case (b/l=0) and normalized by it. As can be seen from Figs. 8 and 9 that he captured only the variation of S_γ from b/l=1/6 to 1 and that manifested a reducing shape function. In the experiments, N_γ increases with B/L as it is given by Meyerhof's relation. Meyerhof deduced this formula simply drawing a linear interpolation line between the bearing capacity at b/l=0 (plane strain case) and b/l=1 (triaxial case). In doing so he considered the variation of peak angle of internal frinction from PSC to TC ($\phi_{PSC}=1.1\phi_{TC}$). And he normalized the bearing capacity al b/l=1 by the bearing capacity at b/l=0 using $\phi_{PSC}=1.1\phi_{TC}$. That is why his equation is running little lower than the point by FEM and model test at b/l=1. These previous formula have been used in the engineering community for a long time, in estimating N_γ for B/L>0.0, based on N_γ for B/L $\geq$0.0, they are conservative, which may increase the cost of construction.

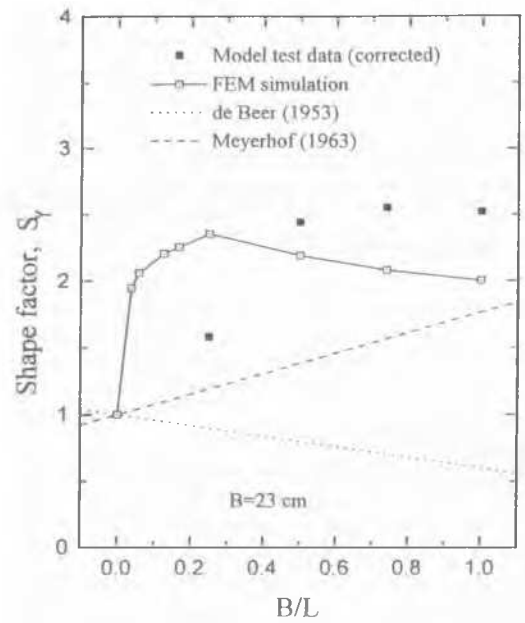

Fig. 8 Effects of shape factors (B_o=23 cm)

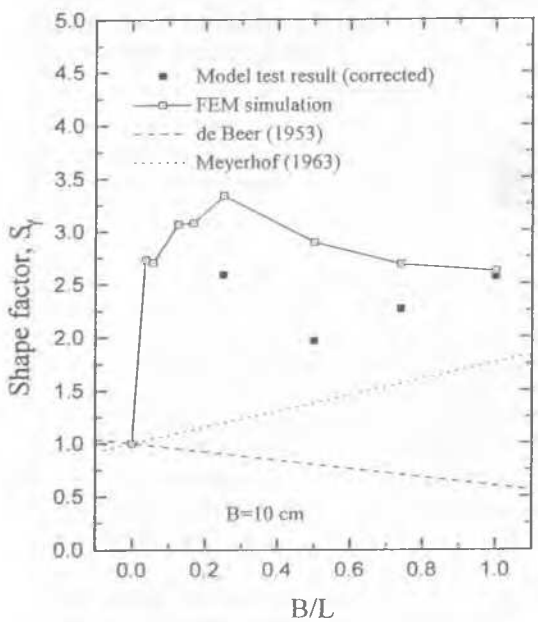

Fig. 9 Effects of shape factors (B_o=10 cm).

5 CONCLUSIONS

1. It has been found that bearing capacity of a footing increase sharply as the ratio B/L increases from zero (plane strain case).
2. There exists an optimum ratio of B/L for which bearing capacity of a rectangular footing can be maximized. The full variation of shape factors with B/L is traced.
3. Opposite trend of semi-empirical formula, given by de-Beer (1970) and Meyerhof (1963) is successfully explained.

REFERENCES

Brinch Hansen J. 1970, A Revised and Extended Formula for Bearing Capacity, *Danish Geotechnical Institute Bulletin* No 28.

de Beer E. E. 1970. Expermental determination of the shape factors and the bearing capacity factors of sand, *Geotechnique* 20, No. 4, pp. 387--411.

Meyerhof G. G. 1963. Some recent research on the bearing capacity of foundations, *Canadian Geotechnical Journal*, 1 (1) : 16--26.

Siddiquee M. S. A. and Tanaka T. and Tatsuoka F. 1995. Tracing the equilibrium path by Dynamic Relaxation in materially nonlinear problems, accepted in *International Journal of Numerical Analysis Methods in Geomechanics.*

Tatsuoka F., Siddiquee M. S. A., Park C.-S., Sakamoto M. and Abe F. 1994. Modelling stress-strain relations of sand, *Soils and Foundations*, Vol. 33, No.2, pp. 60-81.

Vesic Aleksandar S., and Winterkorn H. F. and Fang H. Y. 1973. Bearing Capacity of Shallow Foundations, *Foundation Engineering Handbook.*